COMBINING MULTI-FACETED LABORATORY STUDIES OF 74001-2 AND REGIONAL REMOTE SENSING TO ADDRESS HOW PYROCLASTIC ERUPTIONS RECORD AND AFFECT THE LUNAR VOLATILE BUDGET.

C.K. Shearer[1,2], A. Bell[3], S.B. Simon[1], S. Eckley[4], J. Simon[5], J. Dottin[6], J. Wimpenny[7], L.Gaddis[2], Z. Sharp[1], A. Gargano[2], R.A. Zeigler[5], F. Jourdan[8], A. Cavosie[8], A. Nemchin[8], N. Zellner[9], J. Stopar[2], L. Borg[7], M. Norman[10], P. King[10], C. Menold[9], R.M.G. Armytage[4], W.P. Buckley[4], and J.B. Setera[11]. [1]Institute of Meteoritics, University of New Mexico, Albuquerque, NM 87131; [2]Lunar and Planetary Institute, Houston TX 77058; [3] University of Colorado, Boulder, CO; [4]Jacobs-JETSII, NASA JSC, Houston, TX; [5]ARES, NASA Johnson Space Center, Houston TX 77058-3696, [6]Brown University, Providence, RI 02912; [7]Lawrence Livermore National Laboratory, Livermore CA 94550; [8]Curtin University, Perth, WA 6845 AU; [9]Albion College, Albion, MI 49224; [10]Australian National University, Canberra, ACT 2600 AU; [11]University of Texas at El Paso/Jacobs-JETS II, NASA JSC, Houston, TX. *cshearer@unm.edu*

Introduction: Basaltic magmatism is an efficient process for bringing volatiles from a planetary interior to its surface, with the possibility of generation of a transient lunar atmosphere as abundant volcanic materials degassed [1]. However, pyroclastic deposits are locations where trapped gases may be studied [e.g., 2,3]. Volatile-rich pyroclastic deposits occur over a wide surface area of the Moon [3-5], indicating that the transport of volatiles and associated pyroclastic materials from the Moon's mantle to the surface was a wide-spread phenomenon.

Numerous studies analyzing remotely sensed data and using empirical modeling have demonstrated that various stages of pyroclastic eruptions significantly influence gas release patterns, morphology, and mineralogy of the deposit [3-8]. Many observations based on mare basalts and pyroclastic deposits have identified potential histories of gas release [e.g., 2-10] and their influence on volatiles and their stable isotopes [e.g., 11-13].

The best representation of these pyroclastic deposits in the sample collection is core sample 74001-74002 that was collected during the Apollo 17 mission to the Taurus-Littrow Valley (TLV). The double drive tube penetrated a part of a regional-scale pyroclastic deposit and sampled approximately 68.1 cm of that deposit in the TLV [14]. Remnants of this and other pyroclastic deposits are represented throughout and beyond the TLV [e.g., 14-16]. The stratigraphy of this core has been investigated and defined by numerous studies [9,14,17-20].

The CASA Moon SSERVI research team is conducting a multi-faceted analytical study of this deposit. Data generated from revisiting the stratigraphy of 74001-74002 will be used to place stable isotopes (H, B, Cl, S, Zn, Cu, Rb, Ga, Pb), Ar-Ar and U-Pb chronology, geochemistry, nanometer-scale observations of mineral surfaces, orbital observations, and experiments and modeling within a stratigraphic, eruptive, and geologic context. It is important to place these data into such a context. For example, recent S isotope measurements reported by Dottin et al. [21] show differences within this core that may be related to either changes in source or eruptive process over the course of the eruption (vs. multiple eruptions). A fuller understanding of the stratigraphy is fundamental to resolving this interpretation.

This comprehensive approach can only be achieved within the context of a program such as SSERVI. In addition, imaging produced in this project will be incorporated into a citizen scientist program to further identify many of the textural features of this double drive tube.

Analytical Approach: During the dissection and initial description of 74001-74002 in the mid-1970s [14], the last dissection horizon was epoxy impregnated for the purpose of producing continuous core thin sections. These thin sections are used here to revisit the stratigraphy. High resolution BSE images and X-ray maps (10x10 µm per pixel; Fig. 1) are being obtained using a JEOL JXA-8230 at the University of Colorado. Other images of individual grains and chemical analyses are being made at the University of New Mexico using a JEOL 8200 electron microprobe and a TESCAN Lyra3 SEM. Epoxy-impregnated and sliced samples of the 74001-74002 core are being scanned by X-ray Computed Tomography (XCT) at the Astromaterials X-ray Computed Tomography Lab at Johnson Space Center with a Nikon Metrology XTH320 using a 180 kV microfocus transmission target source (examples are shown in Fig. 1). Scanning conditions were optimized for the size and shape of each sample, but most were scanned at 120 kV and 3.0 W with a voxel size of 12.5 µm.

Initial Results:

Stratigraphy: The stratigraphy of 74001-74002 is determined from 26 rectangular thin sections (4.5 x 2.5 cm) and epoxy-impregnated cores. Fig. 1 illustrates high resolution BSE images of the core from 8 to 13 cm and 15.5 to 20.5 cm depth. Over this interval, the proportion of orange glass beads progressively decreases with increasing depth while the proportion of black beads increases (beads with high proportions of olivine, ilmenite, chromite, and metal). The proportions of orange to black are very discernable in Mg X-ray maps. During this transition, there appears to be limited change in bead size, although the proportion of compound beads increases. Over this interval, the proportion of beads with vesicles does not change. The proportion of coarse (pre-fragmentation) olivine increases with the proportion of orange glass. Using the XCT videos that represent stratigraphy at slightly shallower (~5.5 - 8 cm) and deeper intervals (20.5 – 23 cm) some of these thin section observations

are confirmed. In the future, this 3D perspective will provide some insights into differences, distribution, and orientation of bead shape (teardrop, rod, cylinder).
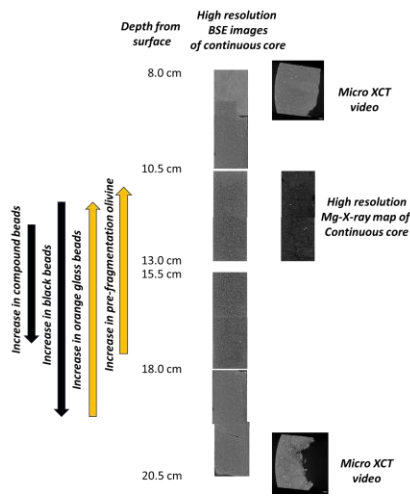

Fig. 1. Examples of data being collected on the 74001-74002 core to be used to reexamine the stratigraphy of the pyroclastic deposit and to be utilized to place petrology (micrometer and nanometer), stable isotopes, and chronology within a geologic-eruptive context.

Variation in volcanic bead composition: There are a variety of pyroclastic melt compositions in the TLV. Delano [17] documented 3 types of high-Ti glasses (74220, Orange I, and Orange II), an intermediate-Ti
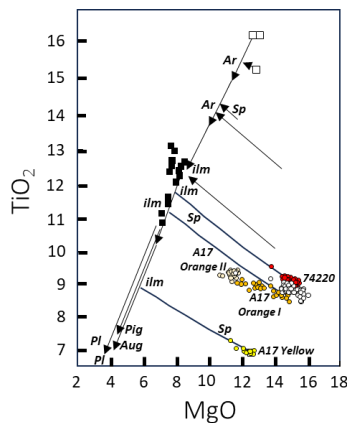

Fig. 2. Plot of TiO_2 vs MgO for orange glasses from the upper portion of 74002 (open circles). Superimposed on this diagram are glass compositions from [17,18] from the TLV. Glass classification scheme by [17] is used here (Orange I, Orange II, Orange 74220, Yellow). The liquid lines of descent determined by [23] are also shown.

melt (Yellow), and a Very Low-Ti melt (VLT). The compositions of the high- and intermediate-melts are presented in Fig. 2. A variety of VLT beads have been identified in the TLV. Further, a detailed study of high-Ti black beads has not been completed to fully discern their relationship to the various orange glass groups. The orange glasses from the TLV are unrelated to the associated crystalline mare basalts [22,23]. Compositions of

orange glasses from the upper portion of the core, where there is a high percentage of orange glass, plot between the 74220 and Orange I glass populations. Analyses of glasses in the core by [9] overlap with these fields. Some care should be taken with this interpretation of our data until we have cross-referenced our data with that of [17]. All these data plot on distinct liquid lines of descent determined by [23].

Summary of new observations: Examining the complete stratigraphy in the continuous thin sections provides further insights into processes for eruption. For example, [9] identified metal droplets occurring in small (<44 μm), post-fragmentation olivine within volcanic beads. This was attributed to shallow (4 km) reduction processes that generated CO during eruption and fragmentation. This is a valid interpretation. However, as shown in Fig. 3, metal droplets also occur in much larger olivine (500 μm) grains that have been previously interpreted as representing pre-fragmentation olivine phenocrysts, potentially residing in the magma chamber [e.g., 2,11,12]. If this interpretation is correct, the olivine-metal assemblage may represent periods of magma chamber degassing prior to eruption or a source region that was metal-saturated.
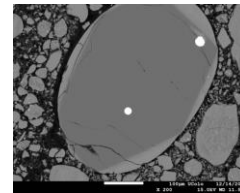

Fig. 3. BSE image of pre-fragmentation olivine (~500μm) with Fe-Ni bleb and a small melt inclusion. This is distinct in occurrence and composition from metal blebs identified by [9].

References: [1] Needham and Kring (2017) EPSL 478, 175-178. [2] Saal et al. (2008) Nature 454, 192-195. [3] Milliken and Li (2017) Nature Geoscience 10, 561-565. [4] Gaddis et al. (1997) LPSC 28th 389. [5] Gaddis et al. (2003) Icarus 161, 262-280. [6] Keske et al. (2020) EPSL 547 116426. [7] Morgan et al. (2021) JVGR 413 107217. [8] Trang et al. (2022) Icarus 375 114837. [9] Weitz et al. (1999) MAPS 34, 527-540. [10] Wilson and Head (2018) GRL 45, 5852-5859. [11] Saal et al. (2021) Science Advances 7(9) eabe4641. [12] Saal et al (2013) Science 340 (6138) 1317-1320. [13] Gargano et al. (2022) Am. Min. 107(11) 1985-1994. [14] Nagle (1978) Drive tubes 74001/74002, Dissection and description. NASA Curation Document. [15] Schmitt (2017) Icarus 298 2-33. [16] Sun et al. (2022) 53rd LPSC abst. #1890. [17] Delano (1986) JGR Solid Earth 91 (B4) 202-213. [18] Shearer et al. (2006) New Views of the Moon 1, 365-518. [19] Heiken and McKay (1978) Proc. LPSC 9th 1933-1943. [20] Pieters (1980) Proc. LPSC 11th 1593-1608. [21] Dottin et al. (2023) JGR Planets 128, no. 2, e2022JE007597. [22] Shearer et al. (2023) New Views of the Moon 2. [23] Longhi (1992) GCA 56, 2235-2251.